ROP16-Mediated Activation of STAT6 Suppresses Host Cell Reactive Oxygen Species Production, Facilitating Type III *Toxoplasma gondii* Growth and Survival

Joshua A. Kochanowsky,[a] Kaitlin K. Thomas,[b] Anita A. Koshy[a,b,c]

[a]Department of Immunobiology, University of Arizona, Tucson, Arizona, USA
[b]BIO5 Institute, University of Arizona, Tucson, Arizona, USA
[c]Department of Neurology, University of Arizona, Tucson, Arizona, USA

ABSTRACT Polymorphic effector proteins determine the susceptibility of *Toxoplasma gondii* strains to IFN-γ-mediated clearance mechanisms deployed by murine host cells. However, less is known about the influence of these polymorphic effector proteins on IFN-γ-independent clearance mechanisms. Here, we show that deletion of one such polymorphic effector protein, ROP16, from a type III background leads to a defect in parasite growth and survival in unstimulated human fibroblasts and murine macrophages. Rescue of these defects requires a ROP16 with a functional kinase domain and the ability to activate a specific family of host cell transcription factors (STAT3, 5a, and 6). The growth and survival defects correlate with an accumulation of host cell reactive oxygen species (ROS) and are prevented by treatment with an ROS inhibitor. Exogenous activation of STAT3 and 6 suppresses host cell ROS production during infection with ROP16-deficient parasites and depletion of STAT6, but not STAT3 or 5a, causes an accumulation of ROS in cells infected with wild-type parasites. Pharmacological inhibition of NOX2 and mitochondrially derived ROS also rescues growth and survival of ROP16-deficient parasites. Collectively, these findings reveal an IFN-γ-independent mechanism of parasite restriction in human cells that is subverted by injection of ROP16 by type III parasites.

IMPORTANCE *Toxoplasma gondii* is an obligate intracellular parasite that infects up to one-third of the world's population. Control of the parasite is largely accomplished by IFN-γ-dependent mechanisms that stimulate innate and adaptive immune responses. Parasite suppression of IFN-γ-stimulated responses has been linked to proteins that the parasite secretes into its host cell. These secreted proteins vary by *T. gondii* strain and determine strain-specific lethality in mice. How these strain-specific polymorphic effector proteins affect IFN-γ-independent parasite control mechanisms in human and murine cells is not well known. This study shows that one such secreted protein, ROP16, enables efficient parasite growth and survival by suppressing IFN-γ-independent production of ROS by human and mouse cells.

KEYWORDS ROP16, STAT transcription factors, *Toxoplasma gondii*, innate immunity, reactive oxygen species

For many microorganisms, differences in virulence between genetically similar strains are driven by polymorphisms that alter or enhance the activity of microbial proteins. *Toxoplasma gondii*, a common obligate intracellular pathogen capable of infecting most warm-blooded mammals, including humans, shows strain-specific differences in virulence (1–4). Acute and chronic infections are usually not harmful to immunocompetent individuals but can result in severe pathology and even death in the immunocompromised (4, 5). While limited evidence suggests that the genotype of

the infecting strain can affect outcomes in humans, these strain-specific differences in outcomes are clearly established in mice (3, 5–13).

Historically, *T. gondii* strains were originally characterized into three clonal lineages (types I, II, and III) based on their acute virulence phenotype in mice (3, 14). Type I strains are highly virulent in laboratory mice, while type II strains exhibit an intermediate virulence, and type III strains are considered avirulent (14). Of the canonical strains, types I and III are more genetically similar compared to type II. Advances in sequencing capabilities have led to *T. gondii* strains now falling into 15 genetic haplotypes of which type I, type II, and type III are now called haplotypes 1, 2, and 3 and clades A, D, and C, respectively (14, 15). Our knowledge of how type I, II, and III strains cause distinct acute disease outcomes in mice has been mapped to differences in the proteins that the parasite secretes into its host cell during and after the invasion process (16–18). These studies also identified several polymorphic proteins that seemed to have no role in lethality of type I strains in mice (19–21). One possibility for the role of these polymorphic proteins is that these strain-specific differences are critical to parasite survival in different, yet-to-be-identified hosts (16). Another possibility is that some of these proteins do not influence disease outcomes of the hypervirulent type I strains but may be critical in the less virulent strains.

One such polymorphic effector protein is rhoptry protein 16 (ROP16). ROP16s from types I, II, and III translocate into the host cell nucleus and have a functional kinase domain, but only the type I and III alleles, which are 99% identical in their amino acid sequence, cause prolonged phosphorylation and activation of STAT3 and 6 and potentially STAT5a (21–24). A single amino acid change in the type II allele of ROP16 renders it incapable of STAT activation (24). In macrophages, the ability of the type I allele of ROP16 to cause prolonged activation of STAT3/6 leads to decreased production of IL-12, a key proinflammatory cytokine involved in generating the IFN-γ response (21, 22). In the context of highly virulent type I strains, ROP16 has only a minimal effect on pathogenesis in mice (21), but ROP16's role in avirulent type III strains has been understudied.

Our group and another recently demonstrated that ROP16 plays a key role in determining the acute and central nervous system (CNS) immune response in mice and is required for efficient type III parasite persistence in mice, possibly by regulating the early immune response (25, 26). During that work, we also identified an IFN-γ-independent *in vitro* growth defect in human fibroblasts in a type III strain that lacked ROP16 (IIIΔ*rop16*). Given this IFN-γ-independent phenotype, we hypothesized that different mechanisms accounted for the *in vivo* and *in vitro* survival defects of the IIIΔ*rop16* strain. Here, we expand on those initial findings by complementing the IIIΔ*rop16* parasites with a series of ROP16 mutants that lack different ROP16 domains/functions. These experiments determined that efficient *in vitro* growth required a functional kinase domain and the ability to phosphorylate STATs. Consistent with these data, the activation of STAT3/6 via cytokine stimulation was sufficient to restore parasite growth in IIIΔ*rop16* parasites. Given the recent finding that type III strains are killed in naive murine macrophages in a reactive oxygen species (ROS)-dependent manner (27), we sought to determine if ROP16 was influencing host cell ROS production in human cells. Indeed, we found that host cells infected with IIIΔ*rop16* parasites accumulated ROS and that pharmacological inhibition of NADPH oxidase 2 (NOX2) and mitochondrially derived ROS restored IIIΔ*rop16* parasites growth to wild-type levels. Finally, using short hairpin RNA (shRNA) knockdown cells and mouse ear tip fibroblasts (mETFs) derived from STAT6 knockout (STAT6KO) mice, we determined that activation of STAT6 was needed for suppression of host cell ROS production and efficient parasite growth and survival. These findings highlight a mechanism by which type III *T. gondii* strains evade IFN-γ-independent cell-autonomous defenses in human and murine cells.

RESULTS

Generation and characterization of IIIΔ*rop16* and ROP16 domain mutants. We previously generated a ROP16-deficient type III strain (IIIΔ*rop16*) and complement (ROP16$_{III}$) using a CRISPR/Cas9-based approach (Fig. 1A) (25). We noted that the
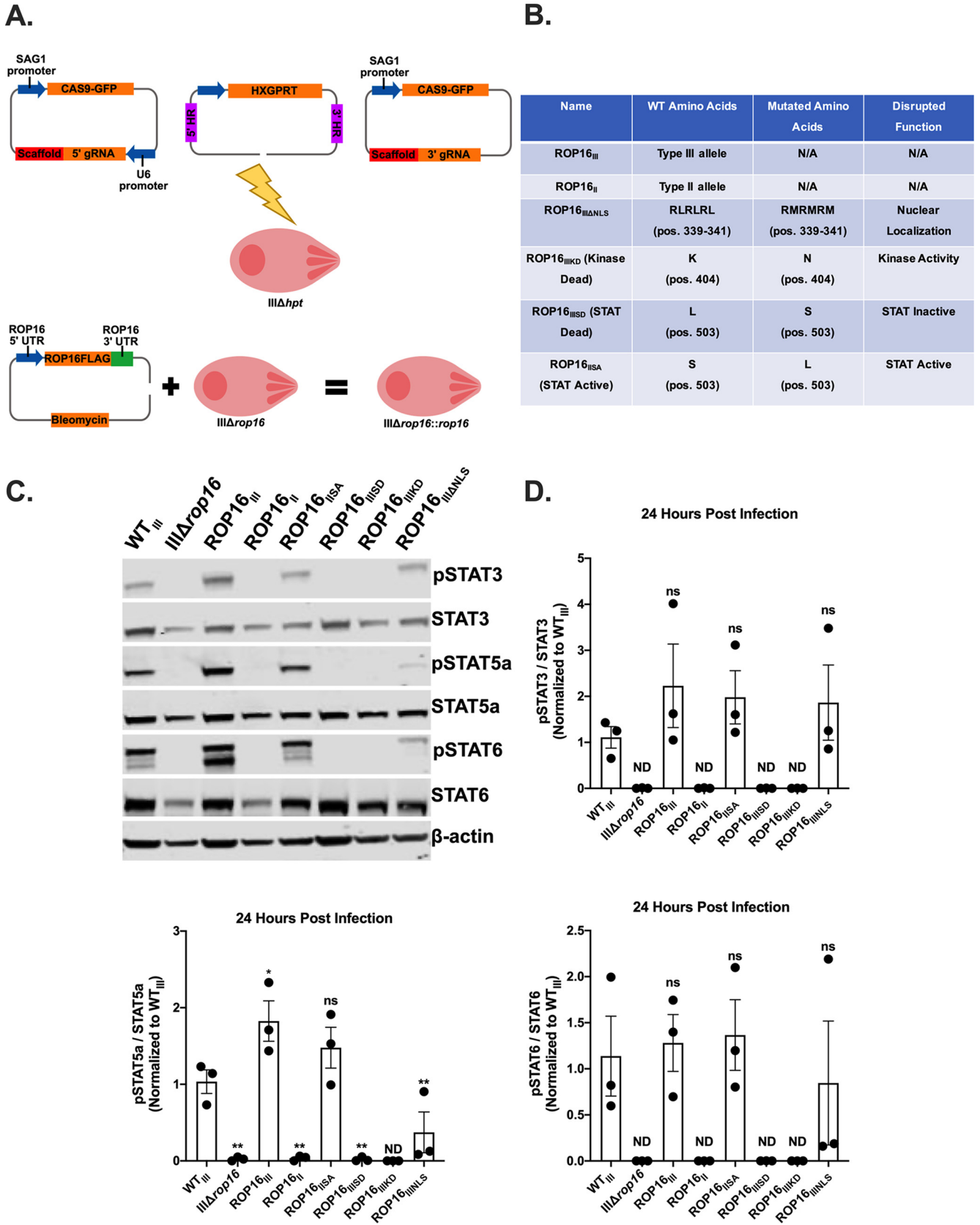
FIG 1 Characterization of ROP16 constructs. (A) Schematic depicting generation of ROP16-expressing strains. Type IIIΔhxgprt parasites were transfected with CRISPR/CAS9 vectors targeting 500 bp upstream (gRNA Up) and downstream (gRNA Down) of the rop16 coding sequence and a linearized vector with

IIIΔ*rop16* strain showed an *in vitro* IFN-γ-independent growth defect, while the *in vivo* deficit related to murine IFN-γ-dependent mechanisms, suggesting that ROP16 might enhance type III parasite fitness in multiple ways (25, 26). To better define this *in vitro* growth defect, we sought to identify which functional domains of ROP16 were required for efficient parasite growth. To accomplish this goal, we generated a series of IIIΔ*rop16* complemented strains, which expressed the type II ROP16 (ROP16$_{II}$), type III ROP16 (ROP16$_{III}$), or domain mutants that were catalytically inactive (ROP16$_{IIIKD}$) or lacked a nuclear localization sequence (ROP16$_{III\Delta NLS}$) (Fig. 1B). Finally, as previous work had demonstrated that a single polymorphic amino acid on ROP16 determined the strain-specific activation of STAT3 and was predicted to determine the activation of STAT5a and 6, we also generated complemented strains that expressed a ROP16$_{III}$ in which the leucine at position 503 was switched to a serine, rendering it "STAT-dead" (ROP16$_{IIISD}$), or expressed a ROP16$_{II}$ in which the serine at position 503 was changed to a leucine, rendering it "STAT-active" (ROP16$_{IISA}$) (Fig. 1B) (24). We validated the deletion and reintroduction of *rop16* in our transgenic strains using a locus-specific PCR that amplifies a 1,000-bp product in the coding sequence of *rop16* (see Fig. S1A in the supplemental material). We confirmed expression of our ROP16 constructs via immunofluorescent (IFA) staining of their engineered FLAG tag (Fig. S1A and B). Finally, we confirmed that our ROP16$_{III\Delta NLS}$-expressing strain was unable to translocate to the nucleus of the host cell (Fig. S1C).

As most work has been done with the type I ROP16 allele, we first sought to confirm that the type III allele also causes prolonged activation of STAT3, 5a, and 6. To that end, we analyzed human foreskin fibroblasts (HFFs) infected with our panel of engineered type III strains (Fig. 1B). As expected, given that the type III allele is 99% identical at the amino acid level (3 to 6 amino acid differences) to the type I allele, wild-type (WT$_{III}$) and ROP16$_{III}$ parasites induced prolonged phosphorylation of STAT3, 5a, and 6 while the IIIΔ*rop16*, ROP16$_{II}$, and ROP16$_{IIIKD}$ strains did not (Fig. 1C and D). Additionally, we found that the single polymorphic amino acid in ROP16 that determines the strain-specific activation of STAT3 also determines activation of STAT5a and STAT6 (Fig. 1C and D). Consistent with prior studies, the lack of an NLS had no effect on STAT3 and 6 phosphorylation but significantly decreased STAT5a phosphorylation (Fig. 1C and D).

Together, these data show that the type III allele of *rop16* is a functional kinase capable of activating STAT3, 5a, and 6. Additionally, the leucine at position 503 dictates the ability of ROP16 to activate not only STAT3 but also STAT5a and STAT6. Finally, mutation of the NLS in ROP16 leads to decreased phosphorylation of STAT5a, but not STAT3 or STAT6.

ROP16 facilitates parasite growth and survival. We previously reported that IIIΔ*rop16* parasites were defective in plaque production *in vitro*, but not in invasion and attachment, indicating a possible defect in parasite growth and survival (25). To further characterize this defect, we performed a plaque assay using our newly generated panel of ROP16 parasites. IIIΔ*rop16*, ROP16$_{II}$, ROP16$_{IIISD}$, and ROP16$_{IIIKD}$ parasites were all defective in forming plaques compared to WT$_{III}$ parasites. ROP16$_{III}$, ROP16$_{IISA}$, and ROP16$_{III\Delta NLS}$ parasites formed plaques at levels comparable to WT$_{III}$ (Fig. 2A).

To test whether this defect in plaque formation was at the level of parasite growth, we infected confluent monolayers of HFFs with our parasite strains and then enumerated the number of parasites per parasitophorous vacuole (PV) at 24 h postinfection (hpi). We found that the ROP16$_{II}$, ROP16$_{IIISD}$, and ROP16$_{IIIKD}$ strains displayed an accumulation of PVs that contained only one parasite compared to WT$_{III}$ parasites,

FIG 1 Legend (Continued)
500-bp regions of homology (HR) to the 5' and 3' untranslated regions (UTRs) of *rop16* surrounding a selectable marker, hypoxanthine-xanthine-guanine phosphoribosyl transferase (HXGPRT). Complementation was achieved using a linearized vector encoding a FLAG-tagged ROP16 construct and a selectable bleomycin resistance marker. (B) Table listing mutations and nomenclature for the ROP16-complemented strains. (C) Representative Western blots from HFFs infected with the identified strains (MOI 5). Protein isolation was done at 24 h postinfection (hpi). (D) Graphs of the densitometry of phosphorylated STAT3/5a/6 normalized to total STAT3/5a/6 Western blots. Bars, mean $\pm$ SEM. Each dot = 1 experiment, n = 3 experiments. One-way ANOVA, Dunnett's multiple-comparison test compared to WT$_{III}$. *, $P \leq 0.05$; **, $P \leq 0.005$. ND = not detected. ns = not significant.
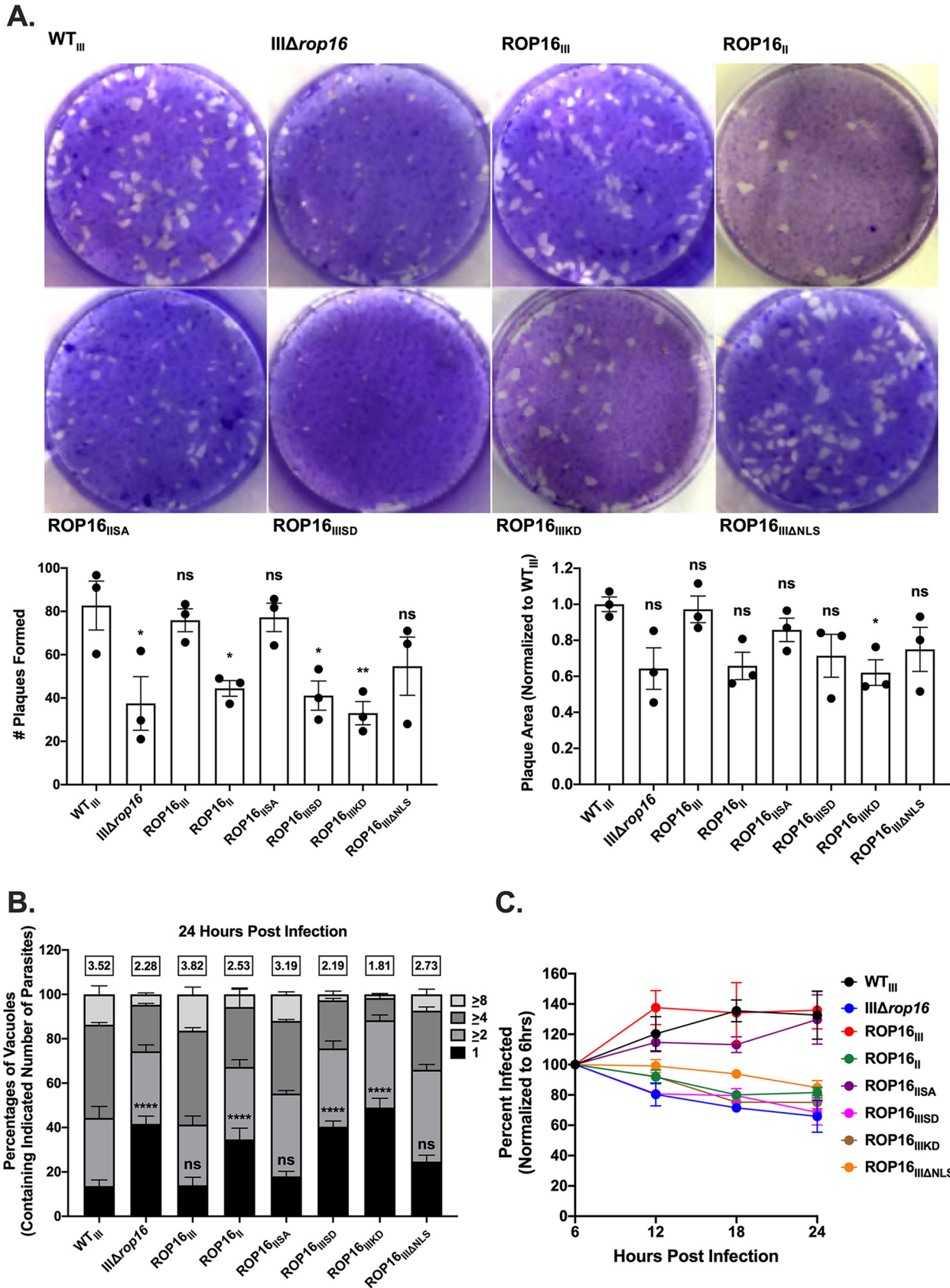
FIG 2 Efficient type III growth and survival requires a ROP16 with an active kinase domain and a leucine at position 503. (A) (Top) Representative images of plaque assays at 10 days postinfection (dpi). HFFs were initially infected with 200 parasites of the identified strains. (Bottom left)

indicating an overall growth defect, while parasites expressing $ROP16_{III}$, $ROP16_{IISA}$, or $ROP16_{III\Delta NLS}$ had WT_{III} levels of growth (Fig. 2B).

As a recent study demonstrated that type III strains are cleared from naive murine bone marrow-derived macrophages (BMDMs) without the need for IFN-γ stimulation (27), we decided to test if our ROP16 strains were being cleared in HFFs. To this end, we infected confluent monolayers of HFFs with our parasites and then fixed and counted the number of infected cells every 6 h for 24 h. We observed a steady accumulation of the percentage of infected cells over 24 h in our WT_{III}, $ROP16_{III}$, and $ROP16_{IISA}$ strains but noticed a significant decrease in the number of infected host cells in our $ROP16_{II}$, $ROP16_{IIISD}$, and $ROP16_{IIIKD}$ strains (~15 to 20% on average) over time, indicating that parasites were being cleared in an IFN-γ-independent manner (Fig. 2C). The $ROP16_{III\Delta NLS}$ strain showed a significant but less pronounced clearance in HFFs (Fig. 2C).

Together, these data indicate that ROP16 is needed for efficient parasite growth and survival *in vitro*. Efficient parasite growth and survival *in vitro* are dependent on kinase activity, and the ability of $ROP16_{IISA}$ to restore these defects suggests that activation of STATs is necessary as well. Interestingly, while the $ROP16_{III\Delta NLS}$-expressing strain had no growth defect, there was a small but significant increase in parasite clearance, indicating that nuclear localization of ROP16 may play a limited role in parasite survival. Finally, we expanded on recent work (25–27) by showing that ROP16 suppresses clearance of type III parasites in unstimulated human fibroblasts.

Type III parasites accumulate ROS in their host cells in a ROP16-dependent manner. IFN-γ exerts its antiparasitic effects at the cellular level by upregulating immunity-related GTPases (IRGs) and guanylate binding proteins (GBPs) that disrupt the PV and lead to eventual clearance of the parasite in mice (28–34). Several other studies have also implicated the IFN-γ-dependent production of nitric oxide and autophagy-related clearance (21, 35, 36). Given that human cells lack the same IRG systems and our observation of an IFN-γ-independent defect in parasite growth and survival, we reasoned that the mechanism of parasite suppression and clearance *in vitro* must be something other than these canonically described IFN-γ-dependent mechanisms.

Prior work demonstrated that host cells infected with type I parasites deficient in ROP16 showed an accumulation of reactive nitrogen species (RNS) in an IFN-γ-dependent manner (21). Given that the type III strain has shown significant differences from the type I strain (25, 26), we sought to determine if IFN-γ-independent RNS production might also be playing a role in the IIIΔ*rop16* survival defect by quantifying RNS levels in host cells. We observed no difference in RNS accumulation among any of our strains in our unstimulated HFFs, indicating that IFN-γ-independent RNS production is not playing a role in the ROP16-dependent clearance we see in HFFs (Fig. S2A).

As a recent study demonstrated that type III parasites are cleared by ROS-dependent and GBP5-dependent mechanisms in naive murine BMDMs (27), we hypothesized that these mechanisms might be involved in the restriction and clearance of IIIΔ*rop16* parasites in HFFs. To test whether GBP5 was involved, we infected confluent monolayers of HFFs, treated with or without IFN-γ, with our parasite strains and quantified the accumulation of GBP5 around parasite-containing vacuoles. At 9 hpi, we detected little GBP5 accumulation around the PV (1 to 3%) regardless of ROP16 status in untreated HFFs (Fig. S2B). Prestimulation with IFN-γ resulted in an increase in GBP5 accumulation around PVs, but ROP16 status did not affect GBP5 localization to the PV (Fig. S2B).

FIG 2 Legend (Continued)
Quantification of plaques formed by identified strains. (Bottom right) Quantification of plaque area relative to WT_{III}. Each dot = 1 experiment, $n = 3$ experiments. Bars, mean $\pm$ SEM. (B) Replication of identified strains at 24 hpi. Percentages of parasite vacuoles containing indicated number of parasites. Numbers above stacked bar graph represent the overall mean number of parasites per vacuole. Bars, mean $\pm$ SEM. $n \geq 100$ vacuoles/well, 3 wells/experiment, 3 experiments. (C) Intracellular survival of identified strains in HFFs shown as percentage of initial infection at 6 hpi. HFFs were infected with parasites (MOI 1) and, at appropriate time points, fixed and stained for SAG1 to detect parasites and wheat germ agglutinin (WGA) to define host cells. Values, mean $\pm$ SEM. $n = 3$ experiments. (A and C) One-way ANOVA. Dunnett's multiple-comparison test compared to WT_{III}. *, $P \leq 0.05$; **, $P \leq 0.005$; ***, $P \leq 0.0005$. ns = not significant. (B) Two-way ANOVA, Dunnett's multiple-comparison test compared to WT_{III}. ****, $P \leq 0.0001$. ns = not significant.

Finally, to test whether ROS played a role in parasite restriction, we infected confluent monolayers of HFFs with our parasite strains, and at 18 hpi, we quantified host cell ROS accumulation via IFA. In cells infected with the IIIΔrop16, ROP16$_{II}$, ROP16$_{IIISD}$, and ROP16$_{IIIKD}$ strains, we observed an increased accumulation of ROS compared to cells infected with WT$_{III}$ parasites (Fig. 3A). Though not statistically significant (P value = 0.3163, 0.3505, 0.2217, and 0.7847, respectively), the uninfected cells in these cultures showed a trend toward an increased accumulation of ROS compared to uninfected cells in cultures with WT$_{III}$ parasites. In ROP16$_{III}$-, ROP16$_{IISA}$-, and ROP16$_{III\Delta NLS}$-infected cultures, infected and uninfected host cells displayed similar levels of ROS accumulation as WT$_{III}$-infected cultures (Fig. 3A).

Given the accumulation of host cell ROS, but not RNS or GBP5, in cultures infected with IIIΔrop16 parasites, we hypothesized that ROS was the major driver of the growth and survival defects in our IIIΔrop16 strain. To test this hypothesis, we pharmacologically inhibited ROS production using a ROS inhibitor, N-acetyl-L-cysteine (NAC), during infection and then quantified parasite growth and survival. Consistent with ROS driving the IIIΔrop16 defects, treatment of HFFs with NAC for 6 or 24 h was sufficient to restore growth of IIIΔrop16 parasites to WT$_{III}$ levels (Fig. 3B). However, only 24-h treatment of NAC was sufficient to restore survival of IIIΔrop16 parasites (Fig. 3C). NAC treatment during IIIΔrop16 infection was also sufficient to reduce ROS to levels comparable to HFFs infected with WT$_{III}$ (Fig. S3). Taken together, these data demonstrate that ROP16-dependent suppression of ROS accumulation is a key mechanism used by type III parasites to avoid clearance by host cells.

ROS-mediated clearance of IIIΔrop16 also occurs in murine macrophage-like cell lines. We next sought to determine if ROP16-mediated ROS accumulation restricted parasites in mouse and human macrophage cell lines. We infected either IC-21s, a mouse macrophage-like cell line (37), or THP1s, a human monocyte cell line (38) that converts to macrophages when treated with 12-O-tetra-decanoylphorbol-13-acetate (TPA) (39), with WT$_{III}$, IIIΔrop16, or ROP16$_{III}$ parasites and measured parasite growth and survival. Similar to our results in HFFs, IIIΔrop16 parasites exhibited a growth defect compared to WT$_{III}$ parasites that could be restored with a 24-h treatment of NAC in both cell lines (Fig. 4A). While infection of IC-21s with WT$_{III}$, IIIΔrop16, or ROP16$_{III}$ resulted in a decrease in parasite survival, only IIIΔrop16 exhibited an increased clearance in this cell type compared to WT$_{III}$, and this increased clearance could be inhibited by treatment with NAC (Fig. 4B). Interestingly, despite IIIΔrop16 exhibiting a growth defect in differentiated THP1s, there was no effect on parasite survival for any of the indicated strains (Fig. 4B). Finally, we quantified ROS accumulation in these cell lines during infection. In keeping with previous results, IC-21s infected with IIIΔrop16 parasites had an increased amount of ROS compared to WT$_{III}$, while differentiated THP1s infected with IIIΔrop16 did not (Fig. 4C). Together, these results indicate that ROP16-dependent suppression of ROS accumulation occurs in murine macrophage-like cells but not in human macrophages differentiated from a monocyte cell line, suggesting that ROP16 effects may vary between hosts and cell types.

Suppression of STAT6 results in accumulation of ROS and a defect in type III parasite growth and survival. Given the ability of ROP16$_{IISA}$ but not ROP16$_{IIISD}$ to restore parasite growth and survival, our data suggested, but did not directly show, that STAT activation was involved in suppressing host cell ROS production. To determine if STAT activation was needed for parasite growth and survival, we prestimulated HFFs with either IL-4 or IL-6 (40–44). Prestimulation of HFFs with either IL-4 or IL-6 resulted in the activation of STAT3 and 6, but not STAT5a (Fig. S4A). Additionally, IL-4 or IL-6 prestimulation of HFFs fully restored growth of IIIΔrop16 to WT$_{III}$ levels but only partially restored parasite survival (Fig. S4B and C). Together, these data indicate that STAT3 and 6 may be required for type III parasite growth and survival, while STAT5a may play a less prominent role.

To determine which STAT was involved in ROS production, we generated STAT3, STAT5a, and STAT6 knockdown HFF cell lines. We transduced HFFs with lentiviral vectors encoding shRNAs targeting STAT3, STAT5a, or STAT6 and then isolated single cells
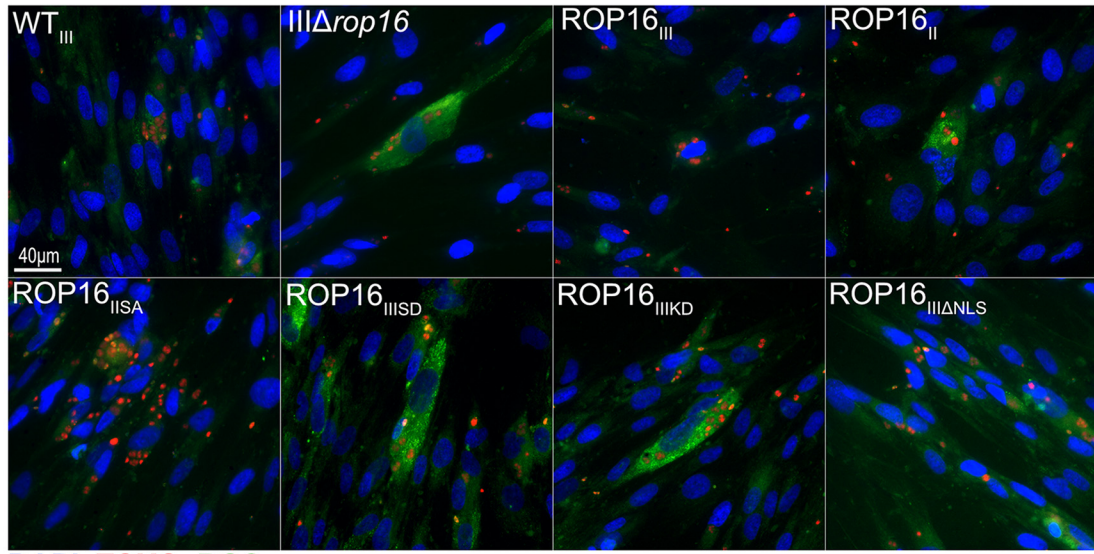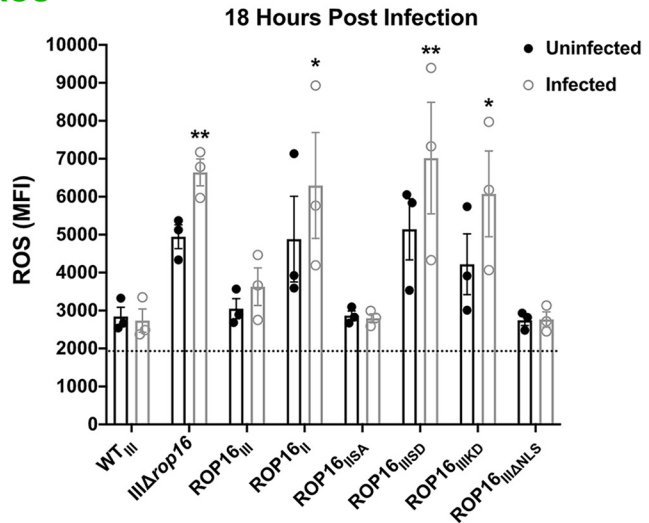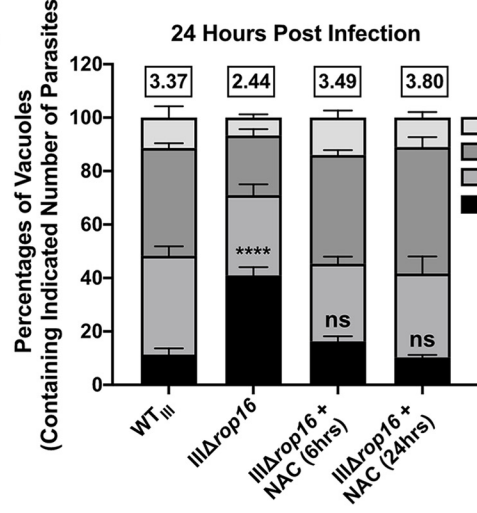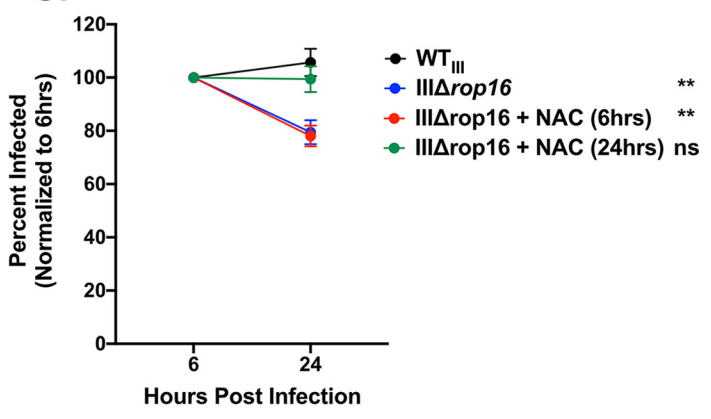
FIG 3 Host cell reactive oxygen species (ROS) restrict intracellular parasites in a ROP16-dependent manner. (A) Representative images of ROS accumulation at 18 hpi in HFFs infected with the identified strains (MOI 1). ROS (green), parasites (red), and nuclei (DAPI stain, blue). Bottom,

to establish clonal cell lines. We used Western blot analysis to determine knockdown efficiency and verify that only the targeted STAT was affected. We achieved knockdown efficiency of up to 60 to 80% of the targeted STAT (Fig. S5). We then tested growth and survival of WT$_{III}$ parasites in these cell lines. Only the STAT6 knockdown cell line showed a growth and survival defect comparable to previous results with IIIΔ*rop16* (Fig. 5A and B). Interestingly, the STAT3 knockdown cells displayed a strong defect in parasite survival but not parasite growth (Fig. 5A and B). This finding is consistent with a recent report demonstrating that early ROP16-independent activation of STAT3 during the invasion process of host cells prevents parasite targeting by autophagy (45). As this finding is ROP16 independent and does not explain the growth defect found in our IIIΔ*rop16* strains, we reasoned that lack of STAT6 activation was more likely to explain the ROS-mediated killing effect in HFFs.

To test whether STAT6 suppression results in ROS accumulation during infection, we infected our knockdown cell lines with WT$_{III}$ parasites and quantified host cell ROS levels. We observed the accumulation of ROS specifically in the STAT6 knockdown cells but not in the STAT3 or STAT5a knockdown cell lines (Fig. 5C). To determine if STAT6-mediated ROS accumulation also played a role in mouse cells, we generated mETFs from STAT6KO mice and infected them with WT$_{III}$ parasites. Deletion of STAT6 from mETFs resulted in a defect in parasite growth and survival and an accumulation of ROS in infected host cells (Fig. 5D to F). Together, these data indicate that activation of STAT6 is required for suppression of host cell ROS production, which enables efficient type III parasite growth and survival in both human and mouse fibroblasts.

Pharmacological suppression of NOX2- and mitochondrially derived ROS is sufficient to restore parasite growth and survival. A recent study demonstrated that type III strains are cleared from naive murine bone marrow-derived macrophages (BMDMs) via NADPH oxidase 2 (NOX2) (27). Additionally, it is known that mitochondrially derived ROS (mROS) are capable of aiding in the clearance of bacteria (46, 47). To test whether NOX2-derived ROS or mROS played a role in parasite restriction, we infected confluent monolayers of HFFs pretreated with either GSK2795039, a NOX2-specific inhibitor (48), or Necrox-5, an mROS scavenger (47), with IIIΔ*rop16* parasites and assayed growth, survival, and ROS generation. Treatment of HFFs with either GSK2795039 or Necrox-5 was sufficient to restore growth and survival of IIIΔ*rop16* parasites to WT$_{III}$ levels (Fig. 6A and B). Additionally, treatment of HFFs with either GSK2795039 or Necrox-5 was sufficient to lower host cell ROS accumulation during IIIΔ*rop16* infection to WT$_{III}$ levels (Fig. 6C). Taken together, these results indicate that both NOX2-derived ROS and mROS play a role in restriction of IIIΔ*rop16* parasites.

DISCUSSION

The data presented here show that one well-studied polymorphic effector protein, ROP16, is responsible for suppressing IFN-γ-independent production of ROS, allowing for efficient parasite growth and survival of an avirulent type III strain of *T. gondii* in HFFs. We have shown that efficient survival of the type III strain during its lytic life cycle in HFFs requires a ROP16 that has a functional kinase domain and can activate STATs. We also observed that ROP16-mediated suppression of ROS occurred in other host backgrounds (mouse) and other cell types (macrophages). Using a combination of cytokine stimulation and HFF STAT knockdown or mETF STAT6KO cell lines, we deter-

FIG 3 Legend (Continued)

quantification of ROS. Each dot = mean ROS value for 1 experiment in the indicated group. $n = 100$ cells/experiment, 3 experiments. Bars, mean ± SEM. Black dotted line indicates the mean ROS value of uninfected controls. MFI, mean fluorescence intensity. (B) Replication of indicated strain in HFFs ± treatment with a ROS inhibitor, N-acetyl-L-cysteine (NAC), for 6 or 24 h during infection. Mean percentages of parasite vacuoles containing indicated number of parasites. Numbers above stacked bar graph represent the overall mean number of parasites per vacuole. Bars, mean ± SEM. $n \geq 100$ vacuoles/well, 3 wells/experiment, 3 experiments. (C) Intracellular survival of identified strain ± treatment with NAC for 6 or 24 h during infection in HFFs expressed as a percentage of initial infection at 6 hpi. HFFs were infected with parasites (MOI 1) and stained as described in the legend to Fig. 2. Values, mean ± SEM. $n = 3$ experiments. (A and C) One-way ANOVA, Dunnett's multiple-comparison test compared to WT$_{III}$. *, $P \leq 0.05$, and **, $P \leq 0.005$. ns = not significant. (B) Two-way ANOVA, Dunnett's multiple-comparison test compared to WT$_{III}$. ****, $P \leq 0.0001$. ns = not significant.
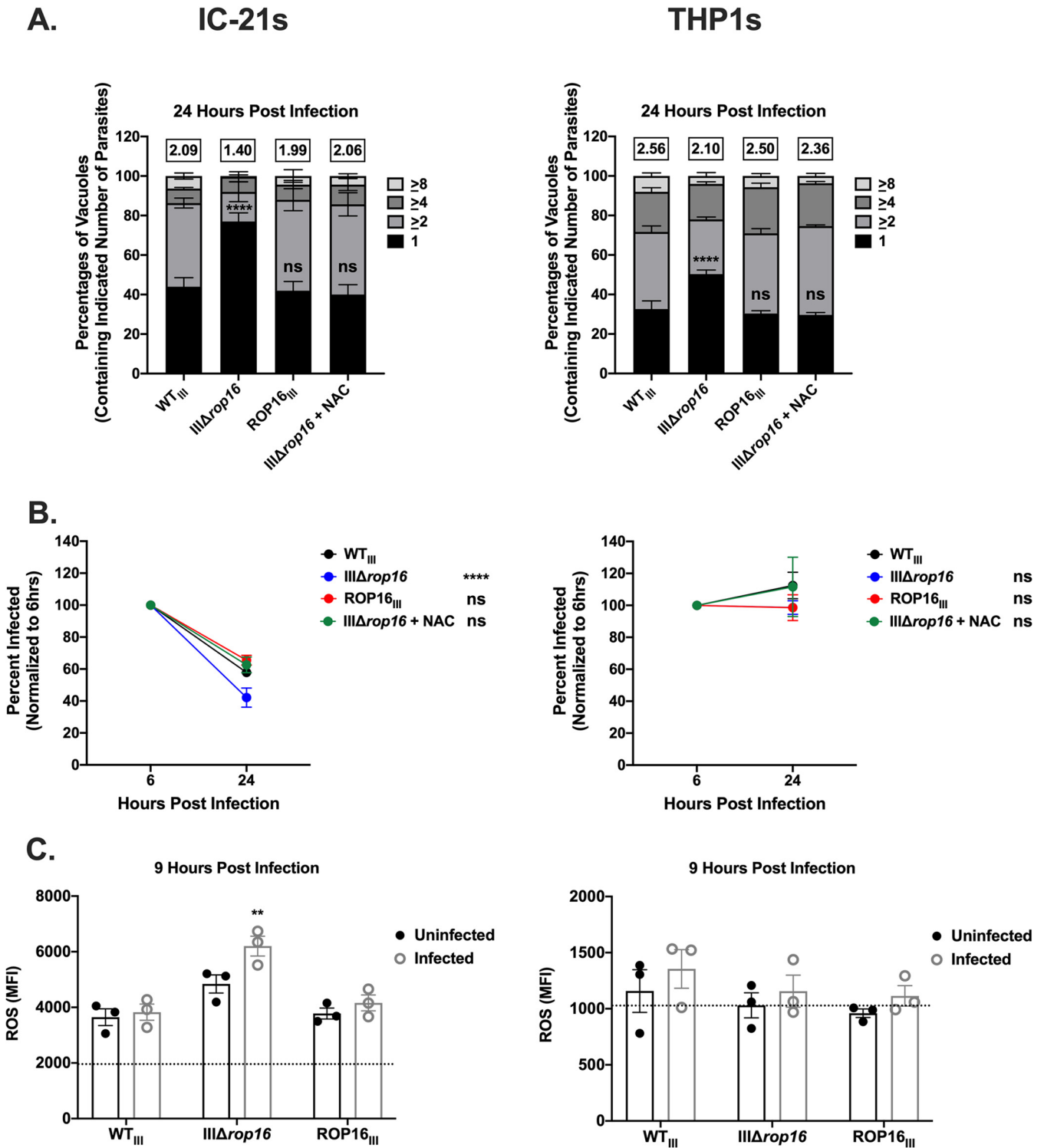
FIG 4 Parasite growth and survival is restricted by ROS in IC-21s but not in differentiated THP1s. (A) Replication of indicated strains in IC-21s and differentiated THP1s ± treatment with NAC for 24 h during infection. Mean percentages of parasite vacuoles containing indicated number of parasites. Numbers above stacked bar graph represent the overall mean number of parasites per vacuole. Bars, mean ± SEM. $n \geq 100$ vacuoles/well, 3 wells/experiment, 3 experiments. (B) Intracellular survival of indicated strains ± treatment with NAC for 24 h during infection of IC-21s and differentiated THP1s expressed as a percentage of initial infection at 6 hpi. HFFs were infected with parasites (MOI 1) and stained as described in the legend to Fig. 2. (C) Quantification of ROS as in Fig. 3. Each dot = mean ROS value for 1 experiment in the indicated group. $n = 100$ cells/experiment, 3 experiments. Bars, mean ± SEM. Black dotted line indicates the mean ROS value of uninfected controls. (A) Two-way ANOVA, Dunnett's multiple-comparison test compared to WT$_{III}$. ****, $P \leq 0.0001$. ns = not significant. (B and C) One-way ANOVA, Dunnett's multiple-comparison test compared to WT$_{III}$. **, $P \leq 0.005$, and ****, $P \leq 0.0001$. ns = not significant.
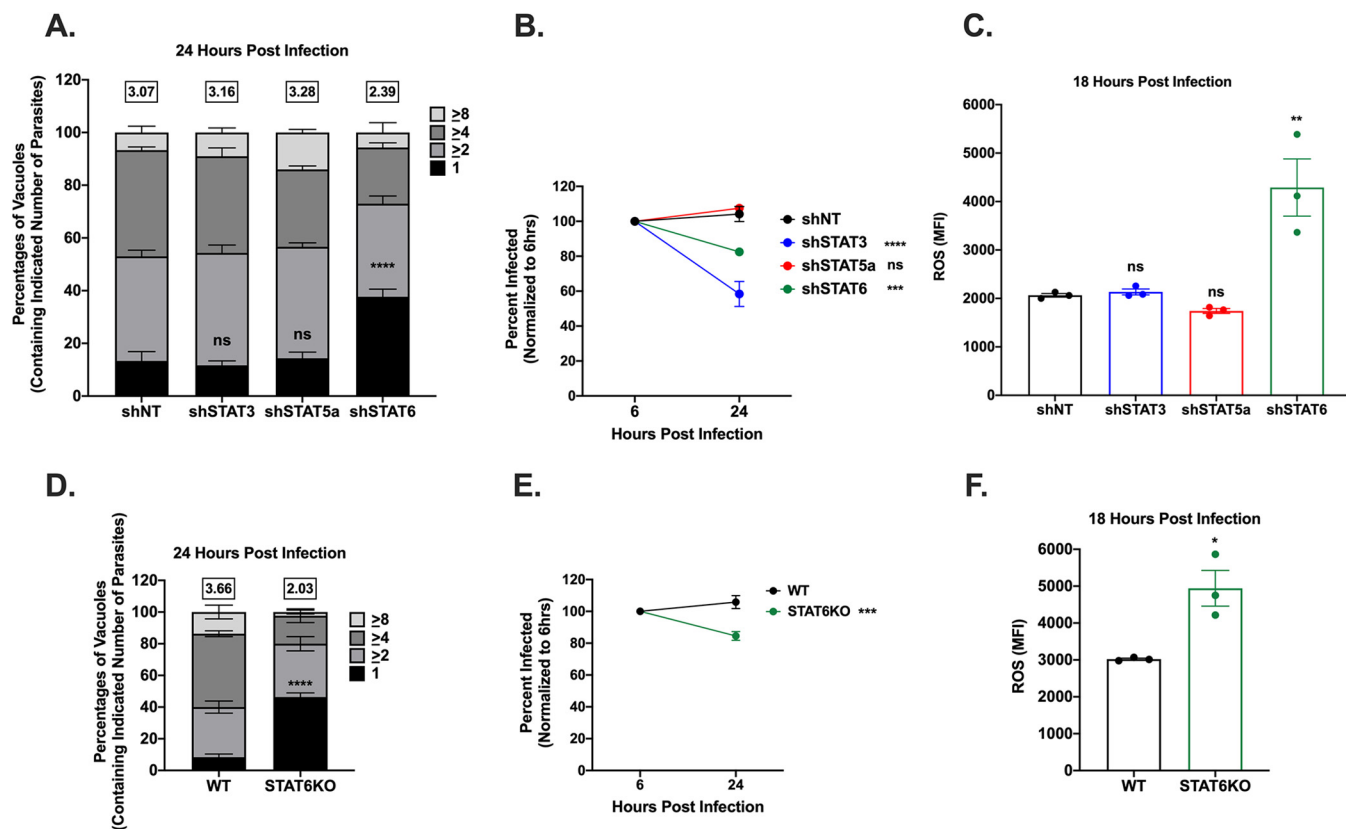
FIG 5 Suppression of STAT6 restricts parasite growth and survival. (A) Replication of WT$_{III}$ in knockdown HFFs at 24 hpi. Mean percentages of parasite vacuoles containing indicated number of parasites. Numbers above stacked bar graph represent the overall mean number of parasites per vacuole. Bars, mean ± SEM. $n \geq 100$ vacuoles/well, 3 wells/experiment, 3 experiments. (B) Intracellular survival of WT$_{III}$ in knockdown HFFs 24 hpi expressed as a percentage of initial infection at 6 hpi. HFFs were infected with parasites and stained as in Fig. 2. Values, mean ± SEM. $n = 3$ experiments. (C) Quantification of ROS in knockdown HFFs. Each dot = mean ROS value for 1 experiment. $n = 100$ cells/experiment, 3 experiments. Bars, mean ± SEM. (D) Replication of WT$_{III}$ in WT or STAT6KO mETFs at 24 hpi. Mean percentages of parasite vacuoles containing indicated number of parasites. Numbers above stacked bar graph represent the overall mean number of parasites per vacuole. Bars, mean ± SEM. $n \geq 100$ vacuoles/well, 3 wells/experiment, 3 experiments. (E) Intracellular survival of WT$_{III}$ in WT or STAT6KO mETFs at 24 hpi expressed as a percentage of initial infection at 6 hpi. HFFs were infected with parasites and stained as in Fig. 2. Values, mean ± SEM. $n = 3$ experiments. (F) Quantification of ROS in WT or STAT6KO mETFs as in Fig. 3. Each dot = mean ROS value for 1 experiment. $n = 100$ cells/experiment, 3 experiments. Bars, mean ± SEM. (A and D) Two-way ANOVA, Dunnett's multiple-comparison test compared to shNT or WT. ****, $P \leq 0.0001$. ns = not significant. (B, C, E, and F) One-way ANOVA, Dunnett's multiple-comparison test compared to shNT or WT. *, $P \leq 0.05$; **, $P \leq 0.005$; ***, $P \leq 0.0005$; ****, $P \leq 0.0001$. ns = not significant.

mined that ROP16-dependent activation of STAT6 is required to abrogate ROS-mediated restriction of type III parasite growth and survival. Finally, using pharmacological inhibitors we showed that both NOX2 and mitochondria are sources of ROS that restrict type III parasites in the absence of ROP16$_{III}$. These findings highlight a role for ROS as an IFN-γ-independent mechanism of parasite control that is suppressed by ROP16$_{III}$ in human cells.

Though we have identified a previously unrecognized role for ROP16 in repression of host cell ROS production, we have not identified what host-parasite interactions trigger the production of ROS that is ultimately suppressed by ROP16$_{III}$. Interestingly, we observed that uninfected cells in these cultures showed a trend toward an increased accumulation of ROS compared to uninfected cells in cultures with WT$_{III}$ parasites. Given that we have previously shown that *T. gondii* injects its rhoptry contents into cells it does not invade (26), these data may indicate that injection of ROP proteins without ROP16 triggers the host cell ROS response. Another possibility is that the actively infected cells release a signal that has a paracrine effect that produces ROS in neighboring uninfected cells.

While we have not determined what host-parasite interactions trigger the production of ROS, we have identified both NOX2 and mitochondria as important sources of ROS generation. NADPH oxidases are known to drive the respiratory burst that kills
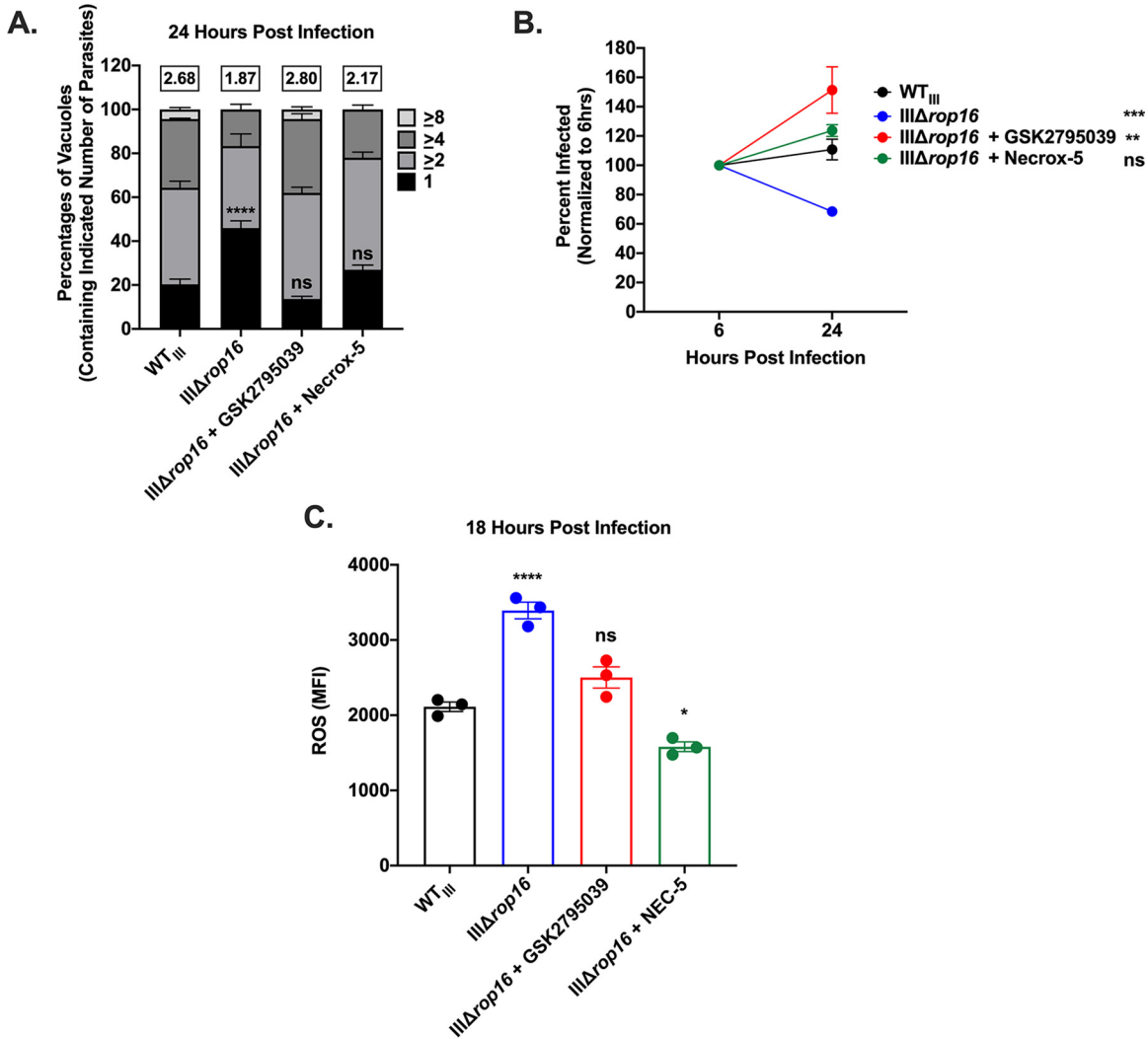
FIG 6 NOX2- and mitochondrially derived ROS restrict parasite growth and survival. (A) Replication of indicated strains in HFFs ± treatment with a NOX2 inhibitor, GSK2795039, or an mROS scavenger, Necrox-5, for 24 h during infection. Mean percentages of parasite vacuoles containing indicated number of parasites. Numbers above stacked bar graph represent the overall mean number of parasites per vacuole. Bars, mean ± SEM. $n \geq 100$ vacuoles/well, 3 wells/experiment, 3 experiments. (B) Intracellular survival of indicated strains ± treatment with GSK2795039 or Necrox-5 for 24 h during infection in HFFs expressed as a percentage of initial infection at 6 hpi. HFFs were infected with parasites (MOI 1) and stained as described in the legend to Fig. 2. Values, mean ± SEM. $n = 3$ experiments. (C) Quantification of ROS as in Fig. 3 in HFFs ± treatment with GSK2795039 or Necrox-5 for 18 h during infection. Each dot = mean ROS value for 1 experiment in the indicated group. $n = 100$ cells/experiment, 3 experiments. Bars, mean ± SEM. (A) Two-way ANOVA, Dunnett's multiple-comparison test compared to WT_{III}. ****, $P \leq 0.0001$. ns = not significant. (B and C) One-way ANOVA, Dunnett's multiple-comparison test compared to WT_{III}. *, $P \leq 0.05$; **, $P \leq 0.005$; ***, $P \leq 0.0005$; and ****, $P \leq 0.0001$. ns = not significant.

phagocytosed pathogens (49). Though we have not performed electron microscopy studies to show the exact mechanism by which the ROS kill parasites, we anticipate that such studies would be consistent with the transmission electron microscopy studies done in a recent paper that implicated NADPH oxidase in the control of intracellular type III parasites in naive murine macrophages (27). The NADPH oxidase-dependent effect in this prior study identified a ROP16-independent effect, highlighting that ROS killing mechanisms may differ between immune cells (macrophages) and non-immune cells (fibroblasts) and between hosts (murine versus human).

Our observation that mROS also played a role in parasite restriction is in keeping with several studies that have shown that mROS plays an important role in macrophage killing of phagosomally localized bacteria (46, 47) and extends this work to suggest that mROS may play in important role in pathogen defense in nonimmune cells as

well. This finding is especially interesting given that type I and III strains, but not type II strains, show high levels of host mitochondrion association with the PV, the host membrane-derived structure, which surrounds intracellular parasites and avoids fusion with the phagolysosome (50–59). Host mitochondria associating with the PV might be able to deliver mitochondrion-derived vesicles harboring ROS (47) to the underlying parasites. Such a mechanism might also partially explain why strains that have host mitochondrial association also retain a ROP16 that can suppress ROS production. Additionally, at least one study has shown that STAT6 colocalizes with mitochondria (60) and thus may have other roles outside of acting as a transcription factor. Future studies will focus on the link between type I and III strains' host cell mitochondrion association and STAT6-dependent suppression of host ROS generation.

While invasion of its host cell and establishment of the PV during *T. gondii* infection are processes that are largely conserved between strains, a growing body of research has shown that the repertoire of secreted effector proteins can have distinct functions between strains such as the activation of STATs by type I and III alleles of ROP16 and NF-κB activation by GRA15 in type II strains (20, 61–64). Notably, type II strains lack a ROP16 that can activate STATs, though it is predicted to have a functional kinase domain (20–24). This difference raises the question of how type II strains avoid ROS-mediated parasite restriction. A few possible explanations include that type II strains might not trigger an ROS response, or they might have a compensatory ROP16-independent mechanism that suppresses ROS production or an increased capacity for tolerating the presence of ROS. Interestingly, type II strains that lack ROP16 show no *in vivo* defect and may even cause an increase in CNS parasite burden (65). Together, these data highlight that host-specific pressures likely influenced the evolution of *T. gondii* strain-specific traits. Type III strains may have evolved to survive in hosts with particularly strong ROS responses. Future work should be directed toward determining what downstream STAT6-regulated genes are involved in blocking ROS production and identifying how differences in ROS production in *T. gondii*'s broad host range affect the survival of different *T. gondii* strains.

MATERIALS AND METHODS

Parasite maintenance. As previously described, all parasite strains used in this study were maintained through serial passage in human foreskin fibroblasts (gift of John Boothroyd, Stanford University, Stanford, CA) using Dulbecco modified Eagle medium (DMEM), supplemented with 10% fetal bovine serum, 2 mM glutagro, and 100 IU/ml penicillin and 100 μg/ml streptomycin (cDMEM). In addition to the strains described below, the previously described type III (CEP), IIIΔ*rop16*, and ROP16$_{III}$ strains expressing mCherry or tdTomato were also used (25).

IC-21 and THP1 cell lines. IC-21s (gift of Janko Nikolich-Zugich, University of Arizona) were maintained in RPMI 1640 + L-glutamine supplemented with 10% fetal bovine serum, and 100 IU/ml penicillin and 100 μg/ml streptomycin prior to downstream experiments. THP1s (gift of Felicia Goodrum, University of Arizona) were maintained in RPMI 1640 + L-glutamine supplemented with 10% fetal bovine serum, 1 mM sodium pyruvate, and 100 IU/ml penicillin and 100 μg/ml streptomycin prior to downstream experiments. THP1 monocyte-macrophage differentiation was induced as previously described prior to downstream experiments (39). Briefly, THP1s were added to glass coverslips on 24-well plates and treated with 100 nM 12-O-tetra-decanoylphorbol-13-acetate (TPA) for 24 h and then replaced with standard growth medium for 48 h, after which the differentiated macrophages were used in downstream experiments.

Generation of plasmids containing ROP16 constructs. All the primers used to make and validate the IIIΔ*rop16* strain are listed in Table S1 in the supplemental material. The ROP16 construct-expressing plasmids were constructed using a previously described FLAG-tagged ROP16-encoding vector and the In-Fusion mutagenesis kit and protocol (Takara, no. 638920) (25).

Generation of ROP16 mutant strains. Generation of IIIΔ*rop16* and ROP16$_{III}$ parasites was previously described (25). For the newly generated strains, IIIΔ*rop16* parasites were transfected with 50 μg of linearized plasmid DNA harboring FLAG-tagged ROP16 constructs and a bleomycin resistance marker. Selection for bleomycin resistance was performed as previously described (25, 66). Post-transfection freshly egressed parasites were resuspended in DMEM supplemented with 50 μg/ml of Zeocin (InvivoGen, 11006-33-0) for 4 h and then added to HFF monolayers supplemented with 5 μg/ml Zeocin to select for integrants. This process was repeated 3 times prior to plating by limiting dilution to isolate single clones. Single clones were subsequently screened by PCR for ROP16 integration (Fig. S1A; PCR primers listed in Table S1).

Immunofluorescence microscopy. For immunofluorescence assays, cells were fixed with 4% paraformaldehyde for 15 min. The cells were then permeabilized and blocked for 60 min with 0.1 to 0.2%

(vol/vol) Triton X-100 in phosphate-buffered saline (PBS) (pH 7.4), typically with 3% (wt/vol) goat serum. For *T. gondii* intracellular growth and survival assays, cells were incubated with mouse polyclonal anti-SAG1 (DG52) (67) at 1:10,000 overnight, followed by incubation with Alexa Fluor 647 secondary antibodies (Molecular Probes) for 1 h. For GBP5 localization assays, cells were incubated with anti-SAG1 (DG52) at 1:10,000 and anti-GBP5 (Cell Signaling Technologies, no. 67798) at 1:500 overnight followed by incubation with Alexa Fluor 647 and Alexa Fluor 488 secondary antibodies (Molecular Probes) for 1 h. For ROP16 localization assays, cells were incubated with anti-SAG1 (DG52) at 1:10,000 and anti-DYKDDDDK (Cell Signaling Technologies, no. 14793) at 1:500 overnight followed by incubation with Alexa Fluor 647 and Alexa Fluor 488 secondary antibodies (Molecular Probes) for 1 h. Coverslips were mounted on slides using Fluoromount G (ThermoFisher, 00-4958-02).

Western blotting. Parasites (multiplicity of infection [MOI] 5) were added to HFFs, and protein was extracted at 24 hpi as previously described (20). Western blot analyses were performed using antibodies specific for total STAT3, STAT5a, and STAT6 and for the phosphorylated forms of STAT3 (phospho-Tyr705), STAT5a (phospho-Tyr694), and STAT6 (phospho-Tyr641) (Cell Signaling Technologies; catalog numbers 9139, 94205, 5397, 9145, 9314, and 56554). Anti-beta-actin was used as a loading control (Cell Signaling Technologies, no. 3700). For cytokine assays, HFFs were treated with 100 ng of recombinant human IL-4 or IL-6 (Sigma-Aldrich numbers I4269 and I2786) for 6 h before protein extraction and Western blot analysis. All blots were imaged on an Odyssey CLx (Li-COR). Densitometry was performed using ImageJ/FIJI as previously described (68).

Plaque assay. Confluent monolayers of HFF cells were infected with 200 tachyzoites of the indicated strains in cDMEM, and cultures were left undisturbed for 10 days to allow for development of plaques, after which the media in the cultures was aspirated, and the cultures were fixed in ice-cold 100% methanol for 10 min. Fixed monolayers were stained with crystal violet for 15 min at room temperature. Stained monolayers were then analyzed by light microscopy at ×4 magnification for the number of plaques in the HFF monolayers.

***T. gondii* intracellular growth assays.** For the growth assay, parasite growth rate was determined using previously described methods which employ a direct parasite-per-vacuole scoring approach (69). Briefly, freshly syringe-lysed parasites (MOI 1) were added to confluent HFF monolayers grown on glass coverslips and spun down at 300 rpm for 1 min. After 1 h, the cultures were then washed to remove non-invaded parasites. At 24 hpi, infected monolayers were fixed, permeabilized, and stained with anti-SAG1 antibodies (as above) and then analyzed by fluorescence microscopy to identify the number of parasites per vacuole. One hundred vacuoles per coverslip were analyzed. For ROS rescue assays, HFFs were treated with either 5 mM N-acetyl-L-cysteine (Abcam, ab139473), 25 μM GSK2795039 (MedChemExpress, 1415925-18-6), or 10 μM Necrox-5 (Cayman Chemical, no. 17278) at the time of infection for either 6 or 24 hpi. Cells were then fixed, stained, and quantified as above. For cytokine rescue assays, HFFs were treated with 100 ng of recombinant human IL-4 or IL-6 (Sigma-Aldrich numbers I4269 and #I2786) at the time of infection to more closely mimic ROP16 injection. Cells were then fixed, stained, and quantified as above.

***T. gondii* intracellular survival assays.** As previously described, freshly syringe-lysed parasites (MOI 1) were added to confluent HFF monolayers grown on glass coverslips (32). Cells were infected for 6 h followed by 3 PBS washes to remove extracellular parasites. Cells were fixed every 6 hpi up to 24 hpi using 4% formaldehyde. Prior to permeabilization, cells were stained with wheat germ agglutinin (ThermoFisher W11261) conjugated to Alexa Fluor 488 according to manufacturer's recommendations. Cells were then permeabilized and stained with anti-SAG1 antibodies and Alexa Fluor 647-conjugated secondary antibody as described above. Images were acquired at 40× on a Leica DMI6000 with a motorized stage, using Leica Application Suite X (LAS X). Data from at least 50 fields of view per experiment were used to calculate the percent decrease in infected cells at various time points versus 6 hpi. For ROS rescue assays, HFFs were treated with either 5 mM N-acetyl-L-cysteine (Abcam, ab139473), 25 μM GSK2795039 (MedChemExpress, 1415925-18-6), or 10 μM Necrox-5 (Cayman Chemical, no. 17278) at the time of infection for either 6 or 24 hpi. Cells were then fixed, stained, and quantified as above. For cytokine rescue assays, HFFs were treated with 100 ng of recombinant human IL-4 or IL-6 (Sigma-Aldrich I4269 and I2786) at the time of infection to more closely mimic ROP16 injection. Cells were then fixed, stained, and quantified as above.

Intracellular ROS/RNS measurement assays. Freshly syringe-lysed parasites (MOI 1) were added to confluent HFF monolayers grown on glass coverslips and allowed to infect for 18 h. Cells were then stained using a commercially available cellular ROS/RNS assay kit (Abcam, ab139473) following the manufacturer's protocol. Cells were then imaged at 40× on a Leica DMI6000 with a motorized stage, using Leica Application Suite X (LAS X). One hundred cells per experiment over 50 fields of view were quantified using ImageJ/FIJI. Briefly, individual cells were selected by using the selection tools and the mean fluorescent intensity per cell was obtained by the measure tool as previously described (70, 71).

GBP5 localization assays. HFF monolayers grown on glass coverslips were treated with or without 100 U of IFN-γ (R&D Systems, 285-MI-100) for 24 h prior to infection. Cells were then infected for 9 h, after which they were fixed using 4% formaldehyde. Cells were then permeabilized and stained as described above. Images were acquired at 40× on a Leica DMI6000 with a motorized stage, using Leica Application Suite X (LAS X). Data from at least 50 fields of view per experiment were used to calculate the percent GBP5 localization around the PV.

Generation of STAT3/5a/6 knockdown cell lines. Vectors encoding shRNA targeting STAT3, STAT5a, and STAT6 and a nontargeting control were acquired from Sigma-Aldrich (SHCLNG-NM_003150-TRCN0000329887, SHCLNG-NM_003152-TRCN0000232134, SHCLNG-NM_003153-TRCN0000274209, and SHC002). HEK-293T cells (gifts of Deepta Bhattacharya, University of Arizona) were transfected with 1 μg of

the respective shRNA-encoding plasmid, 750 ng of psPAX2 packaging plasmid, and 250 ng pMD2.G envelope plasmid (gifts of Felicia Goodrum, University of Arizona) using FuGENE transfection reagent and protocol (Promega, no. TM328). Resultant lentiviral particles were collected and concentrated at 24 and 48 hpi using Lenti-X concentrator reagent and protocol (Clontech, no. 631231). HFFs were transduced with 40 μl of concentrated lentiviral particles, and integrants were selected for with 3 μg of puromycin (InvivoGen, no.ant-pr-1) for 48 h. Cells were subjected to limiting dilution and then expanded prior to Western blot analysis.

Generation of murine fibroblasts. B6.129S2(C)-Stat6^{tm1Gru}/J (STAT6KO) mice were purchased from Jackson Laboratories (stock no. 005977) and bred in the University of Arizona BIO5 Animal Facility in accordance with protocols approved by the University of Arizona Institutional Animal Care and Use Committee. Murine ear tip fibroblasts (mETFs) were generated according to previously described protocols (72). Briefly, 2-mm ear punch biopsy specimens were collected from the pinna of adult mice, submerged in 70% ethanol, and then transferred to mETF culture medium on ice for dissection. Tissue layers were dissected apart, cut into 1-mm by 1-mm pieces, and then transferred to a 6-well gelatin-coated plate containing mETF medium. Tissue pieces were evenly distributed and pressed to the bottom of the wells. Fibroblast outgrowth took approximately 2 weeks to reach confluence, after which mETFs were passaged to 100-mm plates for expansion. mETFs were cultured in DMEM supplemented with 20% fetal bovine serum, 100 IU/ml penicillin, 100 μg/ml streptomycin, 1$\times$ HEPES, and 1$\times$ minimal essential medium with non-essential amino acids. After first passage, culture medium was reduced to 10% fetal bovine serum for line maintenance. To generate WT mETFs, the same procedure was used on ear punch biopsy specimens from C57BL/6 (WT) mice purchased from Jackson Laboratories (stock no. 000664).

Statistical analysis. Graphs were generated and statistical analyses were performed using Prism 8.4.2 software. All experiments were performed at least three independent times, and statistical analyses were conducted on the composite data unless reported otherwise. Unless otherwise specified, the data were analyzed using a one-way analysis of variance (ANOVA) with Dunnett's multiple-comparison test to the control (WT$_{III}$). For *T. gondii* intracellular growth assays, a two-way ANOVA with Dunnett's multiple-comparison test to the control (WT$_{III}$) was used.

Data availability. All relevant data are within the paper and its supplemental material. All strains, primers, and plasmids are available upon request.

SUPPLEMENTAL MATERIAL

Supplemental material is available online only.

FIG S1, EPS file, 1.1 MB.

FIG S2, TIF file, 0.5 MB.

FIG S3, TIF file, 0.3 MB.

FIG S4, TIF file, 0.7 MB.

FIG S5, TIF file, 0.6 MB.

TABLE S1, DOCX file, 0.02 MB.

REFERENCES

1. Suzuki Y. 2002. Immunopathogenesis of cerebral toxoplasmosis. J Infect Dis 186:S234–S240. https://doi.org/10.1086/344276.

2. Carruthers VB. 2002. Host cell invasion by the opportunistic pathogen Toxoplasma gondii. Acta Trop 81:111–122. https://doi.org/10.1016/S0001-706X(01)00201-7.

3. Sibley LD, Boothroyd JC. 1992. Virulent strains of Toxoplasma gondii comprise a single clonal lineage. Nature 359:82–85. https://doi.org/10.1038/359082a0.

4. Wreghitt TG, Gray JJ, Pavel P, Balfour A, Fabbri A, Sharples LD, Wallwork J. 1992. Efficacy of pyrimethamine for the prevention of donor-acquired Toxoplasma gondii infection in heart and heart-lung transplant patients. Transpl Int 5:197–200. https://doi.org/10.1007/BF00336069.

5. Ruskin J, Remington JS. 1976. Toxoplasmosis in the compromised host. Ann Intern Med 84:193. https://doi.org/10.7326/0003-4819-84-2-193.

6. Luft BJ, Remington JS. 1992. Toxoplasmic encephalitis in AIDS. Clin Infect Dis 15:211–222. https://doi.org/10.1093/clinids/15.2.211.

7. Desmonts G, Couvreur J. 1974. Congenital toxoplasmosis. N Engl J Med 290:1110–1116. https://doi.org/10.1056/NEJM197405162902003.

8. Grigg ME, Ganatra J, Boothroyd JC, Margolis TP. 2001. Unusual abundance of atypical strains associated with human ocular toxoplasmosis. J Infect Dis 184:633–639. https://doi.org/10.1086/322800.

9. Ferreira IMR, Vidal JE, de Mattos CDCB, de Mattos LC, Qu D, Su C, Pereira-Chioccola VL. 2011. Toxoplasma gondii isolates: multilocus RFLP-PCR genotyping from human patients in Sao Paulo State, Brazil identified distinct

genotypes. Exp Parasitol 129:190–195. https://doi.org/10.1016/j.exppara.2011.06.002.

10. Dubey JP, Lago EG, Gennari SM, Su C, Jones JL. 2012. Toxoplasmosis in humans and animals in Brazil: high prevalence, high burden of disease, and epidemiology. Parasitology 139:1375–1424. https://doi.org/10.1017/S0031182012000765.

11. Furtado JM, Winthrop KL, Butler NJ, Smith JR. 2013. Ocular toxoplasmosis I: parasitology, epidemiology and public health. Clin Exp Ophthalmol 41:82–94. https://doi.org/10.1111/j.1442-9071.2012.02821.x.

12. Remington JS, McLeod R, Wilson CB, Desmonts G. 2011. Toxoplasmosis, p 918–1041. In Remington JS, Klein JO, Wilson CB, Nizet V, Maldonado YA (ed), Infectious diseases of the fetus and newborn infant, 7th ed. Elsevier Inc, Philadelphia, PA.

13. Boothroyd JC, Grigg ME. 2002. Population biology of Toxoplasma gondii and its relevance to human infection: do different strains cause different disease? Curr Opin Microbiol 5:438–442. https://doi.org/10.1016/s1369-5274(02)00349-1.

14. Sibley LD, Ajioka JW. 2008. Population structure of Toxoplasma gondii: clonal expansion driven by infrequent recombination and selective sweeps. Annu Rev Microbiol 62:329–351. https://doi.org/10.1146/annurev.micro.62.081307.162925.

15. Su C, Khan A, Zhou P, Majumdar D, Ajzenberg D, Dardé ML, Zhu XQ, Ajioka JW, Rosenthal BM, Dubey JP, Sibley LD. 2012. Globally diverse Toxoplasma gondii isolates comprise six major clades originating from a small number of distinct ancestral lineages. Proc Natl Acad Sci U S A 109:5844–5849. https://doi.org/10.1073/pnas.1203190109.

16. Hunter CA, Sibley LD. 2012. Modulation of innate immunity by Toxoplasma gondii virulence effectors. Nat Rev Microbiol 10:766–778. https://doi.org/10.1038/nrmicro2858.

17. Saeij JPJ, Boyle JP, Coller S, Taylor S, Sibley LD, Brooke-Powell ET, Ajioka JW, Boothroyd JC. 2006. Polymorphic secreted kinases are key virulence factors in toxoplasmosis. Science 314:1780–1783. https://doi.org/10.1126/science.1133690.

18. Taylor S, Barragan A, Su C, Fux B, Fentress SJ, Tang K, Beatty WL, El Hajj H, Jerome M, Behnke MS, White M, Wootton JC, Sibley LD. 2006. A secreted serine-threonine kinase determines virulence in the eukaryotic pathogen Toxoplasma gondii. Science 314:1776–1780. https://doi.org/10.1126/science.1133643.

19. Saeij JPJ, Boyle JP, Boothroyd JC. 2005. Differences among the three major strains of Toxoplasma gondii and their specific interactions with the infected host. Trends Parasitol 21:476–481. https://doi.org/10.1016/j.pt.2005.08.001.

20. Saeij JPJ, Coller S, Boyle JP, Jerome ME, White MW, Boothroyd JC. 2007. Toxoplasma co-opts host gene expression by injection of a polymorphic kinase homologue. Nature 445:324–327. https://doi.org/10.1038/nature05395.

21. Butcher BA, Fox BA, Rommereim LM, Kim SG, Maurer KJ, Yarovinsky F, Herbert DR, Bzik DJ, Denkers EY. 2011. Toxoplasma gondii rhoptry kinase ROP16 activates STAT3 and STAT6 resulting in cytokine inhibition and arginase-1-dependent growth control. PLoS Pathog 7:e1002236. https://doi.org/10.1371/journal.ppat.1002236.

22. Jensen KDC, Wang Y, Wojno EDT, Shastri AJ, Hu K, Cornel L, Boedec E, Ong YC, Chien YH, Hunter CA, Boothroyd JC, Saeij JPJ. 2011. Toxoplasma polymorphic effectors determine macrophage polarization and intestinal inflammation. Cell Host Microbe 9:472–483. https://doi.org/10.1016/j.chom.2011.04.015.

23. Jensen KDC, Hu K, Whitmarsh RJ, Hassan MA, Julien L, Lu D, Chen L, Hunter CA, Saeij JPJ. 2013. Toxoplasma gondii rhoptry 16 kinase promotes host resistance to oral infection and intestinal inflammation only in the context of the dense granule protein gra15. Infect Immun 81:2156–2167. https://doi.org/10.1128/IAI.01185-12.

24. Yamamoto M, Standley DM, Takashima S, Saiga H, Okuyama M, Kayama H, Kubo E, Ito H, Takaura M, Matsuda T, Soldati-Favre D, Takeda K. 2009. A single polymorphic amino acid on Toxoplasma gondii kinase ROP16 determines the direct and strain-specific activation of Stat3. J Exp Med 206:2747–2760. https://doi.org/10.1084/jem.20091703.

25. Tuladhar S, Kochanowsky JA, Bhaskara A, Ghotmi Y, Chandrasekaran S, Koshy AA. 2019. The ROP16III-dependent early immune response determines the subacute CNS immune response and type III Toxoplasma gondii survival. PLoS Pathog 15:e1007856. https://doi.org/10.1371/journal.ppat.1007856.

26. Chen L, Christian DA, Kochanowsky JA, Phan AT, Clark JT, Wang S, Berry C, Oh J, Chen X, Roos DS, Beiting DP, Koshy AA, Hunter CA. 2020. The Toxoplasma gondii virulence factor ROP16 acts in cis and trans, and

27. Matta SK, Patten K, Wang Q, Kim BH, Macmicking JD, Sibley LD. 2018. NADPH oxidase and guanylate binding protein 5 restrict survival of avirulent type III strains of Toxoplasma gondii in naive macrophages. mBio 9:e01393-18. https://doi.org/10.1128/mBio.01393-18.

28. Yap GS, Sher A. 1999. Effector cells of both nonhemopoietic and hemopoietic origin are required for interferon (IFN)-γ and tumor necrosis factor (TNF)-α- dependent host resistance to the intracellular pathogen, Toxoplasma gondii. J Exp Med 189:1083–1091. https://doi.org/10.1084/jem.189.7.1083.

29. Zhao YO, Rohde C, Lilue JT, Könen-Waisman S, Khaminets A, Hunn JP, Howard JC. 2009. Toxoplasma gondii and the immunity-related GTPase (IRG) resistance system in mice - a review. Mem Inst Oswaldo Cruz 104:234–240. https://doi.org/10.1590/s0074-02762009000200016.

30. Zhao Y, Ferguson DJP, Wilson DC, Howard JC, Sibley LD, Yap GS. 2009. Virulent Toxoplasma gondii evade immunity-related GTPase-mediated parasite vacuole disruption within primed macrophages. J Immunol 182:3775–3781. https://doi.org/10.4049/jimmunol.0804190.

31. Zhao YO, Khaminets A, Hunn JP, Howard JC. 2009. Disruption of the Toxoplasma gondii parasitophorous vacuole by IFNγ-inducible immunity-related GTPases (IRG proteins) triggers necrotic cell death. PLoS Pathog 5:e1000288. https://doi.org/10.1371/journal.ppat.1000288.

32. Fentress SJ, Behnke MS, Dunay IR, Mashayekhi M, Rommereim LM, Fox BA, Bzik DJ, Taylor GA, Turk BE, Lichti CF, Townsend RR, Qiu W, Hui R, Beatty WL, Sibley LD. 2010. Phosphorylation of immunity-related GTPases by a Toxoplasma gondii-secreted kinase promotes macrophage survival and virulence. Cell Host Microbe 8:484–495. https://doi.org/10.1016/j.chom.2010.11.005.

33. Steinfeldt T, Könen-Waisman S, Tong L, Pawlowski N, Lamkemeyer T, Sibley LD, Hunn JP, Howard JC. 2010. Phosphorylation of mouse immunity-related GTPase (IRG) resistance proteins is an evasion strategy for virulent Toxoplasma gondii. PLoS Biol 8:e1000576. https://doi.org/10.1371/journal.pbio.1000576.

34. Yamamoto M, Okuyama M, Ma JS, Kimura T, Kamiyama N, Saiga H, Ohshima J, Sasai M, Kayama H, Okamoto T, Huang DCS, Soldati-Favre D, Horie K, Takeda J, Takeda K. 2012. A cluster of interferon-γ-inducible p65 GTPases plays a critical role in host defense against Toxoplasma gondii. Immunity 37:302–313. https://doi.org/10.1016/j.immuni.2012.06.009.

35. Chao CC, Anderson WR, Hu S, Gekker G, Martella A, Peterson PK. 1993. Activated microglia inhibit multiplication of Toxoplasma gondii via a nitric oxide mechanism. Clin Immunol Immunopathol 67:178–183. https://doi.org/10.1006/clin.1993.1062.

36. Selleck EM, Orchard RC, Lassen KG, Beatty WL, Xavier RJ, Levine B, Virgin HW, Sibley LD. 2015. A noncanonical autophagy pathway restricts Toxoplasma gondii growth in a strain-specific manner in IFN-γ-activated human cells. mBio 6:e01157-15. https://doi.org/10.1128/mBio.01157-15.

37. Walker WS. 1976. Separate Fc-receptors for immunoglobulins IgG2a and IgG2b on an established cell line of mouse macrophages. J Immunol 116:911–914.

38. Tsuchiya S, Kobayashi Y, Goto Y, Okumura H, Nakae S, Konno T, Tada K. 1982. Induction of maturation in cultured human monocytic leukemia cells by a phorbol diester. Cancer Res 42:1530–1536.

39. Arcangeletti MC, Vasile Simone R, Rodighiero I, De Conto F, Medici MC, Maccari C, Chezzi C, Calderaro A. 2016. Human cytomegalovirus reactivation from latency: validation of a "switch" model in vitro. Virol J 13:179. https://doi.org/10.1186/s12985-016-0634-z.

40. Mosser DM, Edwards JP. 2008. Exploring the full spectrum of macrophage activation. Nat Rev Immunol 8:958–969. https://doi.org/10.1038/nri2448.

41. Takeda H, Tanaka T, Shi W, Matsumoto M, Minami M, Kashiwamura SI, Nakanishi K, Yoshida N, Kishimoto T, Akira S. 1996. Essential role of Stat6 in IL-4 signalling. Nature 380:627–630. https://doi.org/10.1038/380627a0.

42. Kis LL, Gerasimcik N, Salamon D, Persson EK, Nagy N, Klein G, Severinson E, Klein E. 2011. STAT6 signaling pathway activated by the cytokines IL-4 and IL-13 induces expression of the Epstein-Barr virus-encoded protein LMP-1 in absence of EBNA-2: implications for the type II EBV latent gene expression in Hodgkin lymphoma. Blood 117:165–174. https://doi.org/10.1182/blood-2010-01-265272.

43. Johnson DE, O'Keefe RA, Grandis JR. 2018. Targeting the IL-6/JAK/STAT3 signalling axis in cancer. Nat Rev Clin Oncol 15:234–248. https://doi.org/10.1038/nrclinonc.2018.8.

44. Yin Z, Ma T, Lin Y, Lu X, Zhang C, Chen S, Jian Z. 2018. IL-6/STAT3 pathway intermediates M1/M2 macrophage polarization during the development

of hepatocellular carcinoma. J Cell Biochem 119:9419–9432. https://doi.org/10.1002/jcb.27259.

45. Portillo J-AC, Muniz-Feliciano L, Lopez Corcino Y, Lee SJ, Van Grol J, Parsons SJ, Schiemman WP, Subauste CS. 2017. Toxoplasma gondii induces FAK-Src-STAT3 signaling during infection of host cells that prevents parasite targeting by autophagy. PLoS Pathog 13:e1006671. https://doi.org/10.1371/journal.ppat.1006671.

46. West AP, Brodsky IE, Rahner C, Woo DK, Erdjument-Bromage H, Tempst P, Walsh MC, Choi Y, Shadel GS, Ghosh S. 2011. TLR signalling augments macrophage bactericidal activity through mitochondrial ROS. Nature 472:476–480. https://doi.org/10.1038/nature09973.

47. Abuaita BH, Schultz TL, O'Riordan MX. 2018. Mitochondria-derived vesicles deliver antimicrobial reactive oxygen species to control phagosome-localized Staphylococcus aureus. Cell Host Microbe 24:625–636.e5. https://doi.org/10.1016/j.chom.2018.10.005.

48. Hirano K, Chen WS, Chueng ALW, Dunne AA, Seredenina T, Filippova A, Ramachandran S, Bridges A, Chaudry L, Pettman G, Allan C, Duncan S, Lee KC, Lim J, Ma MT, Ong AB, Ye NY, Nasir S, Mulyanidewi S, Aw CC, Oon PP, Liao S, Li D, Johns DG, Miller ND, Davies CH, Browne ER, Matsuoka Y, Chen DW, Jaquet V, Rutter AR. 2015. Discovery of GSK2795039, a novel small molecule NADPH oxidase 2 inhibitor. Antioxid Redox Signal 23:358–374. https://doi.org/10.1089/ars.2014.6202.

49. Thomas DC. 2017. The phagocyte respiratory burst: historical perspectives and recent advances. Immunol Lett 192:88–96. https://doi.org/10.1016/j.imlet.2017.08.016.

50. Mordue DG, Håkansson S, Niesman I, Sibley LD. 1999. Toxoplasma gondii resides in a vacuole that avoids fusion with host cell endocytic and exocytic vesicular trafficking pathways. Exp Parasitol 92:87–99. https://doi.org/10.1006/expr.1999.4412.

51. Zhao Y, Marple AH, Ferguson DJP, Bzik DJ, Yap GS. 2014. Avirulent strains of Toxoplasma gondii infect macrophages by active invasion from the phagosome. Proc Natl Acad Sci U S A 111:6437–6442. https://doi.org/10.1073/pnas.1316841111.

52. Sibley LD, Weidner E, Krahenbuhl JL. 1985. Phagosome acidification blocked by intracellular Toxoplasma gondii. Nature 315:416–419. https://doi.org/10.1038/315416a0.

53. Suss-Toby E, Zimmerberg J, Ward GE. 1996. Toxoplasma invasion: the parasitophorous vacuole is formed from host cell plasma membrane and pinches off via a fission pore. Proc Natl Acad Sci U S A 93:8413–8418. https://doi.org/10.1073/pnas.93.16.8413.

54. Mordue DG, Desai N, Dustin M, Sibley LD. 1999. Invasion by Toxoplasma gondii establishes a moving junction that selectively excludes host cell plasma membrane proteins on the basis of their membrane anchoring. J Exp Med 190:1783–1792. https://doi.org/10.1084/jem.190.12.1783.

55. Pernas L, Adomako-Ankomah Y, Shastri AJ, Ewald SE, Treeck M, Boyle JP, Boothroyd JC. 2014. Toxoplasma effector MAF1 mediates recruitment of host mitochondria and impacts the host response. PLoS Biol 12:e1001845. https://doi.org/10.1371/journal.pbio.1001845.

56. Jones TC, Hirsch JG. 1972. The interaction between Toxoplasma gondii and mammalian cells: II. The absence of lysosomal fusion with phagocytic vacuoles containing living parasites. J Exp Med 136:1173–1194. https://doi.org/10.1084/jem.136.5.1173.

57. Adomako-Ankomah Y, English ED, Danielson JJ, Pernas LF, Parker ML, Boulanger MJ, Dubey JP, Boyle JP. 2016. Host mitochondrial association evolved in the human parasite Toxoplasma gondii via neofunctionalization of a gene duplicate. Genetics 203:283–298. https://doi.org/10.1534/genetics.115.186270.

58. Blank ML, Parker ML, Ramaswamy R, Powell CJ, English ED, Adomako-Ankomah Y, Pernas LF, Workman SD, Boothroyd JC, Boulanger MJ, Boyle JP. 2018. A Toxoplasma gondii locus required for the direct manipulation of host mitochondria has maintained multiple ancestral functions. Mol Microbiol 108:519–535. https://doi.org/10.1111/mmi.13947.

59. English ED, Boyle JP. 2018. Impact of engineered expression of mitochondrial association factor 1b on Toxoplasma gondii Infection and the host response in a mouse model. mSphere 3:e00471-18. https://doi.org/10.1128/mSphere.00471-18.

60. Khan R, Lee JE, Yang YM, Liang FX, Sehgal PB. 2013. Live-cell imaging of the association of STAT6-GFP with mitochondria. PLoS One 8:e55426. https://doi.org/10.1371/journal.pone.0055426.

61. Rosowski EE, Lu D, Julien L, Rodda L, Gaiser RA, Jensen KDC, Saeij JPJ. 2011. Strain-specific activation of the NF-κB pathway by GRA15, a novel Toxoplasma gondii dense granule protein. J Exp Med 208:195–212. https://doi.org/10.1084/jem.20100717.

62. Gov L, Karimzadeh A, Ueno N, Lodoen MB. 2013. Human innate immunity to Toxoplasma gondii is mediated by host caspase-1 and ASC and parasite GRA15. mBio 4:e00255-13. https://doi.org/10.1128/mBio.00255-13.

63. Wang P, Li S, Zhao Y, Zhang B, Li Y, Liu S, Du H, Cao L, Ou M, Ye X, Li P, Gao X, Wang P, Jing C, Shao F, Yang G, You F. 2019. The GRA15 protein from Toxoplasma gondii enhances host defense responses by activating the interferon stimulator STING. J Biol Chem 294:16494–16508. https://doi.org/10.1074/jbc.RA119.009172.

64. Sangaré LO, Yang N, Konstantinou EK, Lu D, Mukhopadhyay D, Young LH, Saeij JPJ. 2019. Toxoplasma GRA15 activates the NF-κB pathway through interactions with TNF receptor-associated factors. mBio 10:e00808-19. https://doi.org/10.1128/mBio.00808-19.

65. Fox BA, Rommereim LM, Guevara RB, Falla A, Hortua Triana MA, Sun Y, Bzik DJ. 2016. The Toxoplasma gondii rhoptry kinome is essential for chronic infection. mBio 7:e00193-16. https://doi.org/10.1128/mBio.00193-16.

66. Messina M, Niesman I, Mercier C, Sibley LD. 1995. Stable DNA transformation of Toxoplasma gondii using phleomycin selection. Gene 165:213–217. https://doi.org/10.1016/0378-1119(95)00548-K.

67. Burg JL, Perelman D, Kasper LH, Ware PL, Boothroyd JC. 1988. Molecular analysis of the gene encoding the major surface antigen of Toxoplasma gondii. J Immunol 141:3584–3591.

68. Gallo-Oller G, Ordoñez R, Dotor J. 2018. A new background subtraction method for Western blot densitometry band quantification through image analysis software. J Immunol Methods 457:1–5. https://doi.org/10.1016/j.jim.2018.03.004.

69. Fox BA, Falla A, Rommereim LM, Tomita T, Gigley JP, Mercier C, Cesbron-Delauw MF, Weiss LM, Bzik DJ. 2011. Type II Toxoplasma gondii KU80 knockout strains enable functional analysis of genes required for cyst development and latent infection. Eukaryot Cell 10:1193–1206. https://doi.org/10.1128/EC.00297-10.

70. Li H, Gao A, Feng D, Wang Y, Zhang L, Cui Y, Li B, Wang Z, Chen G. 2014. Evaluation of the protective potential of brain microvascular endothelial cell autophagy on blood-brain barrier integrity during experimental cerebral ischemia-reperfusion injury. Transl Stroke Res 5:618–626. https://doi.org/10.1007/s12975-014-0354-x.

71. Liu B, Huang X, Li Y, Liao W, Li M, Liu Y, He R, Feng D, Zhu R, Kurihara H. 2019. JS-K, a nitric oxide donor, induces autophagy as a complementary mechanism inhibiting ovarian cancer. BMC Cancer 19:645. https://doi.org/10.1186/s12885-019-5619-z.

72. Merritt JK, Collins BE, Erickson KR, Dong H, Neul JL. 2020. Pharmacological read-through of R294X Mecp2 in a novel mouse model of Rett syndrome. Hum Mol Genet 29:2461–2470. https://doi.org/10.1093/hmg/ddaa102.